







Cite this: *J. Mater. Chem. C*, 2017, 5, 4388

Received 24th March 2017,
Accepted 20th April 2017

DOI: 10.1039/c7tc01241a

rsc.li/materials-c

Influence of nanoscale order–disorder transitions on the magnetic properties of Heusler compounds for spintronics†

J. Karel,  ^{‡*} J. E. Fischer,  ^a S. Fabbrici, ^b E. Pippel, ^c P. Werner, ^c M. Vinicius Castergnaro, ^d P. Adler, ^a S. Ouardi, ^a B. Balke, ^e G. H. Fecher,  ^a J. Morais,  ^d F. Albertini, ^b S. S. P. Parkin ^c and C. Felser ^a

Modifications in nanoscale chemical order are used to tune the magnetic properties, namely T_C , of $\text{Co}_2\text{FeSi}_x\text{Al}_{1-x}$ ($0 < x < 1$). High-angle annular dark field scanning transmission electron microscopy (HAADF-STEM) with Z-contrast reveals nanoscale regions of L_{21} order within a B2 matrix in the off-stoichiometry samples. Perhaps surprisingly, the latter, more chemically disordered structure, exhibits a higher T_C . Upon annealing, the off-stoichiometry samples become more homogeneous with the fraction of L_{21} order decreasing. The short-range order was also investigated using X-ray absorption fine structure (XAFS) measurements at the Co and Fe K edges. Since the local atomic environments of Co atoms in the L_{21} and B2 structures are identical, the features presented in the Co K edge XAFS data are the same in both cases. By contrast, the L_{21} and B2 structures exhibit different signatures at the Fe K edge owing to the different chemical environments. Fitting of these spectra confirms the nanoscale chemical disorder observed by HAADF-STEM and the expected role this disorder plays on T_C . Our results point to a methodology that might be extended to modify the magnetic and electronic properties of any Heusler compound; chemical disorder can be an engineering tool to realize highly tailored properties.

Introduction

Increasingly challenging materials requirements for spintronics applications have initiated research efforts towards designing new materials with carefully tailored properties.^{1,2}

The requirements for spin transfer torque (STT) applications are a perfect example, where an ideal candidate material possesses high spin polarization, low saturation magnetization, a high magnetic Curie temperature (T_C), uniaxial magnetic anisotropy and low Gilbert damping.¹ One commonly used design concept is valence electron counting (*via* chemical composition). Heusler compounds are a particularly attractive class of materials from this perspective.² In the full Heusler X_2YZ compounds, the X, Y and Z chemical species can be easily substituted to control the magnetic and electronic properties over a very large parameter space. Additionally, chemical disorder, despite it typically being viewed as detrimental, has also been proposed as an engineering tool for spintronic materials. For instance, Chadov *et al.* showed theoretically that chemical disorder in Mn_3Ga -based Heusler compounds can lead to spin-selective electron localization, which produces enhanced spin polarization.³

In the work presented here, we use changes in nanoscale chemical order to modify the magnetic properties of $\text{Co}_2\text{FeSi}_x\text{Al}_{1-x}$ ($0 < x < 1$). This composition series was chosen for study since both end members, Co_2FeSi and Co_2FeAl , display technologically useful properties, such as high T_C , low damping and half metallicity.^{4–9} Co_2FeSi crystallizes in the L_{21} structure shown in Fig. 2c while Co_2FeAl typically presents partial chemical order (B2 order) shown in Fig. 2d. The Fermi energy (E_F) is near the top (bottom) of the minority states gap in Co_2FeAl (Co_2FeSi), and, consequently, disorder can eliminate the half-metallic behavior.⁴ Thus, our study is focused on the off-stoichiometry compositions in this series where E_F can be shifted to the middle of the minority states gap, thus making the spin-polarization more robust to disorder.¹⁰ In this composition range, chemical disorder can then be used to tune the properties, namely T_C which is crucially important in maintaining stability in spintronic devices. We will show that B2 structured Co_2FeAl exhibits a T_C of 1218 K, which is higher than previously reported.¹¹ In the off-stoichiometry samples, high-angle annular dark field scanning transmission electron microscopy (HAADF-STEM) with Z-contrast reveals nanoscale

^a Max Planck Institute for Chemical Physics of Solids, Dresden, Germany

^b Institute of Materials for Electronics and Magnetism, Parma, Italy

^c Max Planck Institute of Microstructure Physics, Halle, Germany

^d Departamento de Física, Instituto de Física, Universidade Federal do Rio Grande do Sul (UFRGS), Porto Alegre, RS, Brazil

^e Institut für Anorganische und Analytische Chemie, Johannes Gutenberg-Universität, Mainz, Germany

† Electronic supplementary information (ESI) available. See DOI: 10.1039/c7tc01241a

‡ Present address: Department of Materials Science and Engineering, Monash University, Clayton, Victoria, Australia. E-mail: julie.karel@monash.edu

puddles of $L2_1$ order within a B2 matrix. Perhaps surprisingly, the latter, more chemically disordered structure, exhibits a higher T_C . Upon annealing, the off-stoichiometry samples become more homogeneous with the fraction of $L2_1$ order decreasing. Hence a simple annealing procedure to induce chemical disorder on the nanoscale can be used to enhance T_C in a regime where the spin-polarization should be robust to disorder. Our results suggest a similar methodology to modify the magnetic properties can be employed in thin films, where disorder can be introduced during growth.

Experimental procedure

The compounds $\text{Co}_2\text{FeSi}_x\text{Al}_{1-x}$ with $x = 0, 0.2, 0.4, 0.6, 0.8$ and 1.0 were synthesized by arc-melting stoichiometric quantities of the pure elements (purity at least 99.999+%) under an argon atmosphere. The ingots were remelted three times to improve the homogeneity. For annealing, the ingots were sealed in a tantalum tube, which was encapsulated in a quartz ampoule. Co_2FeSi was annealed at 1000°C for 21 days, Co_2FeAl was annealed at 900°C for 10 days and the off-stoichiometric compositions were annealed at 730°C for 7 days; all samples were subsequently quenched in a mixture of water and ice. Samples were characterized using X-ray diffraction, scanning electron microscopy/wavelength dispersive X-ray spectroscopy (SEM/WDX), ^{57}Fe Mössbauer spectrometry, SQUID magnetometry and AC magnetic susceptibility using thermomagnetic analysis (TMA). HAAD-STEM with Z-contrast and X-ray absorption fine structure (XAFS) were measured on samples with composition $\text{Co}_2\text{FeSi}_{0.2}\text{Al}_{0.8}$ annealed at 730°C for 7 days. Further details of the sample preparation and characterization can be found in the ESI.†

Results and discussion

X-ray diffraction patterns do not indicate any impurity phases and show the compounds become more B2-like with increasing Al content, as revealed by a gradual reduction in the intensity of the (111) peak. ^{57}Fe Mössbauer spectrometry shows only one Fe sextet for each sample, indicating a lack of Co–Fe disorder. SEM/WDX analysis reveals average compositions that agree well with the target compositions and no indication of impurity phases. Further details of the sample characterization are given in the ESI.†

The total magnetic moment per formula unit m at 2 K as a function of the number of valence electrons (N_{VE}) is shown in Fig. 1a. All the samples (except Co_2FeAl) closely follow the Slater–Pauling rule represented by the solid black line, indicating half-metallic ferromagnetism.¹² Co_2FeAl has the B2 structure, and its deviation from Slater–Pauling behavior has been previously reported and ascribed to this partial chemical disorder.⁴ The fact that m varies only by changing the non-magnetic Z element is well understood by the Slater–Pauling rule, which fixes the Fermi energy in the minimum (band gap) of the minority electron density of states. Thus, the number of

occupied minority electrons is also fixed, and a change in the number of valence electrons can only result in a change in the number of majority electrons, independent of what atom they reside on. Finally, the magnetic moment in the primitive cell is just given by the difference in the number of majority and minority electrons.

Fig. 1a also shows a decrease in T_C of nearly 200 K with an increase of only 1 valence electron; this behavior is in contradiction to the theoretically predicted and experimentally observed trends in Co_2 -based Heusler materials where T_C tends to increase with increasing N_{VE} .^{13,14} However, these predictions and observations were shown over a much larger range of N_{VE} and in compounds with the $L2_1$ structure, whereas here the Al

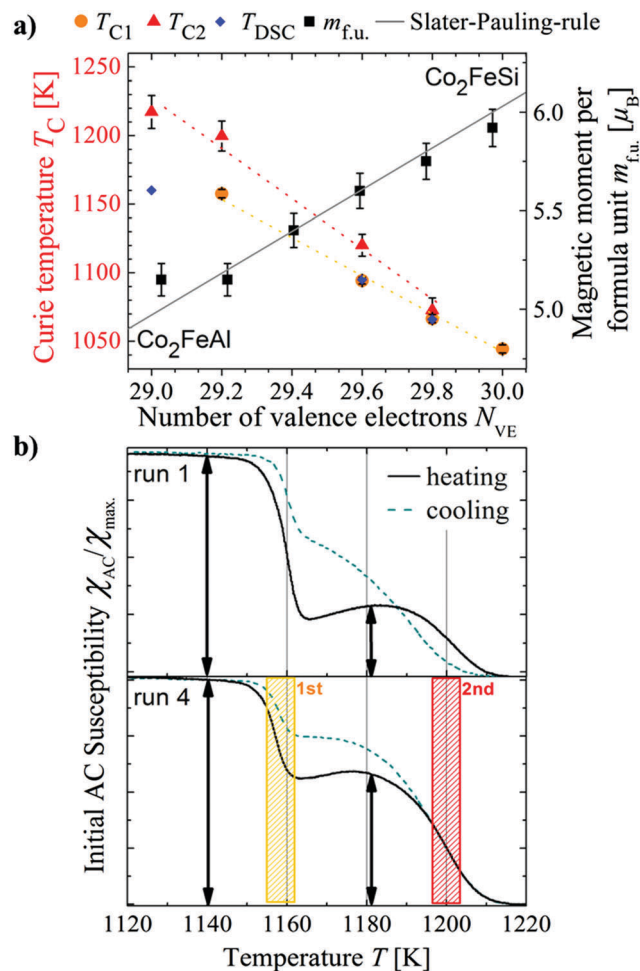


Fig. 1 (a) Curie temperature, transition temperatures observed in the DSC measurement and magnetic moment per formula unit as a function of the number of valence electrons. (b) Examples of TMA measurements on one piece of the sample $\text{Co}_2\text{FeSi}_{0.2}\text{Al}_{0.8}$. The upper picture shows the first measurement on a virgin sample, below the fourth measurement carried out on the same piece is depicted. The relative intensity of the second transition grows with increased number of heating and cooling cycles until reaching an equilibrium state in which the transition temperature and the transition's intensity remain stable. The values shown for the T_C in Table S1 (ESI†) and (a) are determined from the equilibrium signal. Once this equilibrium is reached, the differences between the transition temperatures in the heating and cooling curves disappear.



containing members of the series partly or completely exhibit the B2 structure. Evidently, the degree of order in the sample is the more important factor when studying the trend in the T_C over such a small range in N_{VE} . In addition, the off-stoichiometry samples exhibit two transition temperatures (Fig. 1b), originating from two separate magnetic phases. The endpoints of the composition range, by contrast, present a single magnetic transition temperature, with Co_2FeAl demonstrating the highest reported T_C of 1218 K.

Fig. 1b displays susceptibility measurements after 4 annealing cycles for $x = 0.2$; one cycle consists of heating and cooling slowly from 300 K to 1226 K. These curves show that after annealing, the magnetic phase with the higher T_C

grows. The lower transition temperature corresponds to endothermic transitions below the melting point found in differential scanning calorimetry measurements and to magnetic transition temperatures found by other groups.^{11,15,16} The second transition has not been observed before and does not correspond to structural transition temperatures found by Umetsu *et al.*¹¹

To probe the origin of these separate transitions, two samples of $\text{Co}_2\text{FeSi}_{0.2}\text{Al}_{0.8}$ were studied in detail. One sample (#1) was synthesized and annealed using the procedure described above. A second sample (#2), from the same ingot as #1, was additionally heated and cooled slowly four times between room temperature and 1226 K, to simulate the

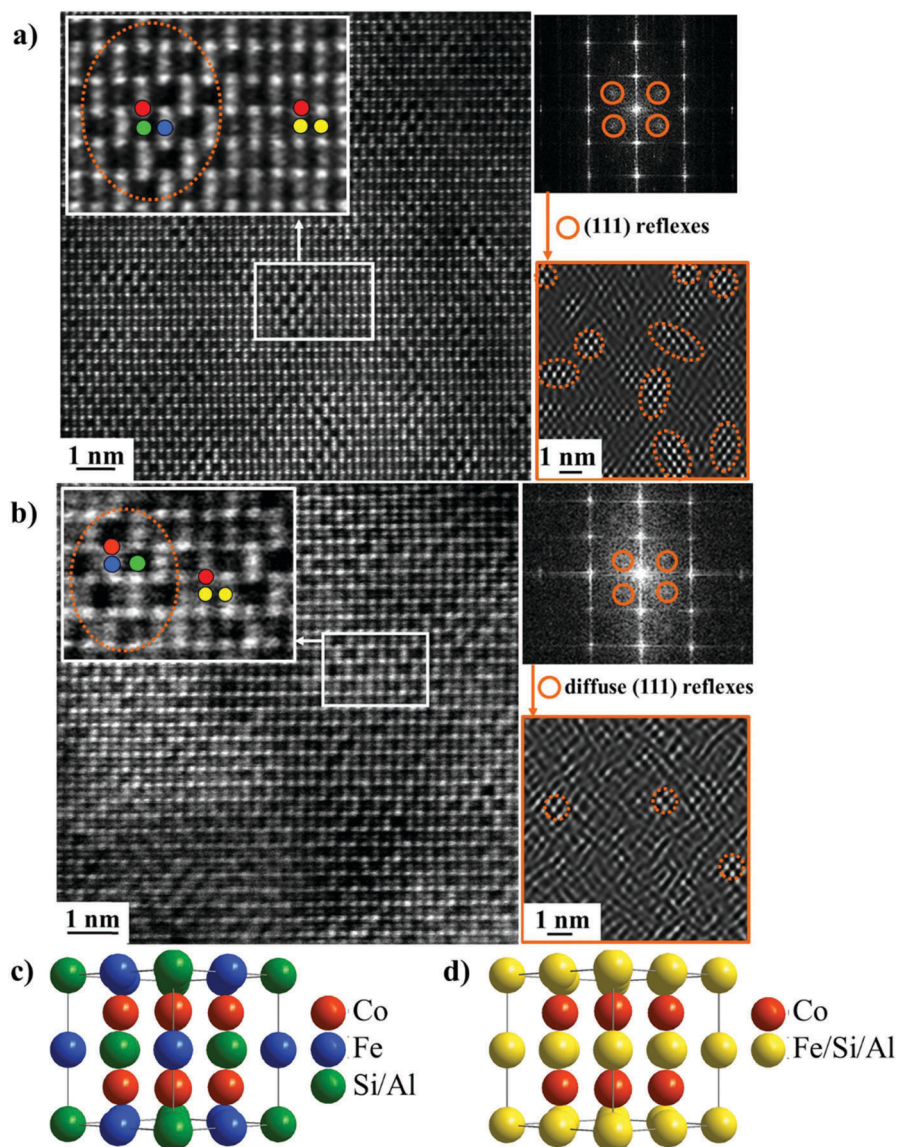


Fig. 2 High-angle annular dark field scanning transmission electron microscopy (Z-contrast) images of $\text{Co}_2\text{FeSi}_{0.2}\text{Al}_{0.8}$, (a) on an as-prepared sample, (b) on a sample that was heated and cooled four cycles in the TMA apparatus. The zone axis is (110) in both cases. Bright spots correspond to a higher mass density (Co, Fe) darker spots correspond to atoms with lower mass density (Al, Si), example atoms are marked with the colors used for L_{21} ordered structure (c) and B2 type structure (d). Adding the filtered information from the red encircled (111) reflexes in the diffraction pattern to the raw image highlights areas with high order which produced the (111) reflexes (dashed orange circles).



conditions in the TMA apparatus. HAADF-STEM (Z-contrast) images were taken along the (110) zone axis (Fig. 2a and b). Filtering these images using the (111) reflections leads to the highlighted $L2_1$ ordered areas (orange circles in Fig. 2a and b). A sharp contrast exists between the $L2_1$ ordered areas and the B2 areas in sample #1, and we assign the transitions observed in the AC susceptibility curves to the Curie temperatures of the $L2_1$ (T_{C1}) and B2 (T_{C2}) phases based on these results. The first transition is sharper, and the second transition is broadened, which is consistent with T_{C1} corresponding to the ordered phase, while T_{C2} originates from the phase with more chemical disorder. Upon annealing (sample #2), the fraction of the $L2_1$ phase decreases, and the contrast between the $L2_1$ and B2 phases is not as sharp. This observation suggests a homogenization of the structure, which is more B2-like after annealing.

The short-range order was also investigated using XAFS measurements at the Co and Fe K edges. In this case, a new sample was prepared following the same synthesis route and annealing as was done for samples #1 and #2. The main structural parameters were obtained by fitting the Fourier transforms (FT) of the extended X-ray absorption fine structure (EXAFS) signals at both edges (see ESI†). Since the local atomic environments of Co atoms in the $L2_1$ and B2 structures are identical, the features presented in the Co K edge EXAFS data will be the same in both cases. By contrast, the $L2_1$ and B2 structures present different signatures at the Fe K edge owing to the different chemical environments, which lead to distinct photoelectron scattering processes within the sample and, thus, distinct EXAFS signals.

FEFF 9.6¹⁷ was used to calculate the scattering amplitudes and phase shifts resulting from the photoelectron scattering processes in both the B2 and $L2_1$ structures for Co_2FeZ . The best fits of the FTs of samples #1 and #2 at the Co and Fe edges are presented in Fig. 3a and b, respectively, and the structural parameters obtained from this analysis are given in Table S3 and S4 of the ESI†. The coordination numbers obtained for both samples are in agreement with those expected for Fe in Co_2FeZ in a B2 structure, despite small variations in the Fe:Z

ratio at longer distances. For sample #1, the number of Z atoms as second nearest neighbors was 13% higher than expected for a perfect B2 structure, and the number of Fe atoms at the same distance was 16% lower. Moreover, the number of Z atoms as third nearest neighbors was 7% lower than expected for a perfect B2 structure, and the number of Fe atoms was 10% higher. These modifications in the local environment surrounding the Fe atoms indicate that some fraction of Fe is present in the $L2_1$ structure in sample #1. The changes are less evident at longer distances than at the shorter ones, indicating the presence of small islands of Co_2FeZ with the $L2_1$ structure dispersed in the predominant B2 matrix. In sample #2, the EXAFS analysis pointed to a smaller contribution of $L2_1$ structure compared to sample #1. These results are consistent with the nanoscale chemical disorder observed by HAADF-STEM and the expected role this disorder plays on the modifications in T_C . An increase in T_C with introduced chemical disorder was recently observed in $\text{Co}_{1+x}\text{Fe}_{2-x}\text{Si}$ Heusler compounds; namely the largest T_C was reported for the $\text{Co}_{1.5}\text{Fe}_{1.5}\text{Si}$ composition.¹⁸ Analysis of the Fe local atomic environments *via* Mössbauer spectroscopy indicated that a change in the site occupancy and resultant modification of the exchange energies (due to variations in the magnetic moment and exchange integrals) was the likely origin of the enhanced T_C . Similarly, the greater T_C observed here is likely related to the modifications in the local atomic environments in the B2 structure with respect to the $L2_1$ structure.

Nanoscale chemical disorder could present further opportunities to engineer functional materials and realize new properties. For instance, recent work has reported ultrafast demagnetization in amorphous CoFeB due to enhanced spin-lattice scattering resulting from structural disorder.¹⁹ The methodology presented in our work might therefore be extended to engineer materials with carefully tailored nanoscale chemical disorder for use in all optical magnetic switching. Moreover, control of chemical disorder can lead to the discovery of new materials properties, such as the giant intrinsic exchange bias reported in Mn-Pt-Ga as a result of anti-site disorder.²⁰

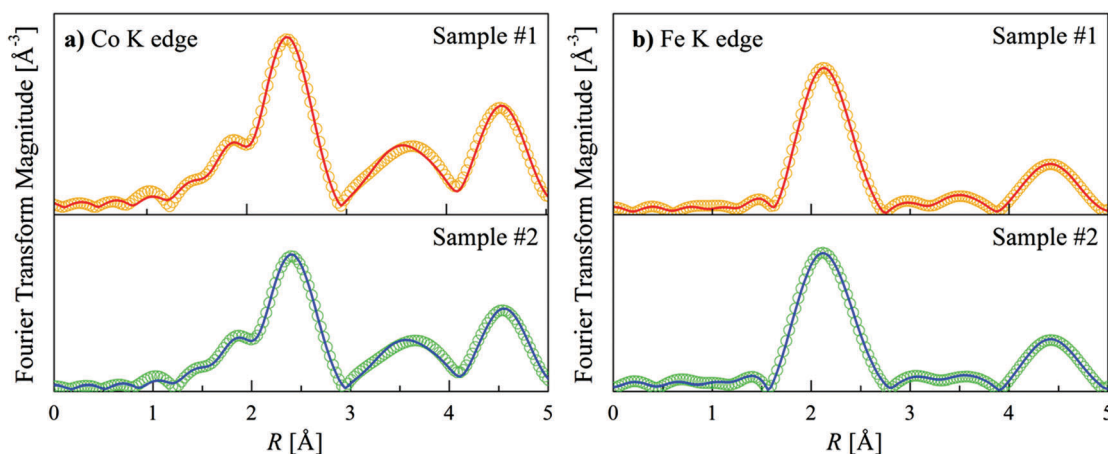


Fig. 3 Magnitudes of the Fourier transforms at the (a) Co and (b) Fe edges. In both subfigures, the red and blue lines indicate the fit, and the orange and green open circles display the experimental data.



Conclusion

In summary, modifications in T_C in off-stoichiometry $\text{Co}_2\text{FeSi}_x\text{Al}_{1-x}$ ($0 < x < 1$) compounds result from nanoscale chemical disorder. This composition range was specifically examined since the spin-polarization should be more robust to disorder. HAAD-STEM and EXAFS revealed $L2_1$ ordered nano-puddles in a B2 matrix in the as-prepared sample with $x = 0.2$; the fraction of B2 chemical order grew after annealing, resulting in an enhanced T_C . Moreover, we present a record T_C of 1218 K for B2-structured Co_2FeAl . Our results point to a methodology that might be extended to modify the magnetic and electronic properties of any Heusler compound, thin film or bulk; chemical disorder can be an engineering tool to realize highly tailored properties.

Acknowledgements

The authors gratefully acknowledge support of this work by the Brazilian Synchrotron Light Laboratory (proposals XPD-17015 and XAFS1-17012), CNPq and CAPES-PROBRAL.

References

- 1 J. Winterlik, S. Chadov, A. Gupta, V. Alijani, T. Gasi, K. Filsinger, B. Balke, G. H. Fecher, C. A. Jenkins, F. Casper, J. Kueler, G.-D. Liu, L. Gao, S. S. P. Parkin and C. Felser, *Adv. Mater.*, 2012, **24**, 6283.
- 2 T. Graf, C. Felser and S. S. P. Parkin, *Prog. Solid State Chem.*, 2011, **39**, 1.
- 3 S. Chadov, S. W. D'Souza, L. Wollmann, J. Kiss, G. H. Fecher and C. Felser, *Phys. Rev. B: Condens. Matter Mater. Phys.*, 2015, **91**, 094203.
- 4 T. M. Nakatani, A. Rajanikanth, Z. Gercsi, Y. K. Takahasi, K. Inomata and K. Hono, *J. Appl. Phys.*, 2007, **102**, 033916.
- 5 Q. L. Ma, X. M. Zhang, T. Miyazaki and S. Mizukami, *Sci. Rep.*, 2015, **5**, 7863.
- 6 T. Kubota, S. Tsunegi, M. Oogane, S. Mizukami, T. Miyazaki, H. Naganuma and Y. Ando, *Appl. Phys. Lett.*, 2009, **94**, 122504.
- 7 S. Mizukami, D. Watanabe, M. Oogane, Y. Ando, Y. Miura, M. Shirai and T. Miyazaki, *J. Appl. Phys.*, 2009, **105**, 07D306.
- 8 M. Belmeguenai, M. S. Gabor, T. Petrisor, Jr., F. Zighem, S. M. Cherif and C. Tiusan, *J. Appl. Phys.*, 2015, **117**, 023906.
- 9 H. C. Herper, B. Krumme, D. Ebke, C. Antoniak, C. Weis, A. Warland, A. Hütten, H. Wende and P. Entel, *J. Appl. Phys.*, 2011, **109**, 07E128.
- 10 G. H. Fecher and C. Felser, *J. Phys. D: Appl. Phys.*, 2007, **40**, 1582.
- 11 R. Y. Umetsu, A. Okubo and R. Kainuma, *J. Appl. Phys.*, 2012, **111**, 073909.
- 12 I. Galanakis, P. H. Dederichs and N. Papanikolaou, *Phys. Rev. B: Condens. Matter Mater. Phys.*, 2002, **66**, 174429.
- 13 J. Kübler, G. H. Fecher and C. Felser, *Phys. Rev. B: Condens. Matter Mater. Phys.*, 2007, **76**, 024414.
- 14 G. H. Fecher, H. C. Kandpal, S. Wurmehl, C. Felser and G. Schönhense, *J. Appl. Phys.*, 2006, **99**, 08J106.
- 15 X. Zhu, Y. Dai and C. Luo, *J. Magn. Magn. Mater.*, 2016, **398**, 7.
- 16 B. Balke, G. H. Fecher and C. Felser, *Appl. Phys. Lett.*, 2007, **90**, 242503.
- 17 J. J. Rehr, J. J. Kas, F. D. Vila, M. P. Prange and K. Jorissen, *Phys. Chem. Chem. Phys.*, 2010, **12**, 5503.
- 18 J. E. Fischer, J. Karel, S. Fabbrici, P. Adler, S. Ouardi, G. H. Fecher, F. Albertini and C. Felser, *Phys. Rev. B*, 2016, **94**, 024418.
- 19 S. Bonetti, M. C. Hoffmann, M.-J. Sher, Z. Chen, S.-H. Yang, M. G. Samant, S. S. P. Parkin and H. A. Dürr, *Phys. Rev. Lett.*, 2016, **117**, 087205.
- 20 A. K. Nayak, M. Nicklas, S. Chadov, P. Khuntia, C. Shekhar, A. Kalache, M. Baenitz, Y. Skourski, V. K. Guduru, A. Puri, U. Zeitler, J. M. D. Coey and C. Felser, *Nat. Mater.*, 2015, **14**, 679.

